Dear author,

Please note that changes made in the online proofing system will be added to the article before publication but are not reflected in this PDF.

We also ask that this file not be used for submitting corrections.

Deep-Sea Research II ∎ (∎∎∎∎) ∎∎∎–∎∎∎

Contents lists available at ScienceDirect

Deep-Sea Research II

journal homepage: www.elsevier.com/locate/dsr2

Dissolved organic matter dynamics in surface waters affected by oil spill pollution: Results from the Serious Game exercise

M Gonnelli [a], Y Galletti [a], E Marchetti [a], L Mercadante [a], S Retelletti Brogi [a], A Ribotti [b], R Sorgente [b], S Vestri [a], C Santinelli [a]

[a] Consiglio Nazionale delle Ricerche, IBF, Pisa, Italy
[b] Consiglio Nazionale delle Ricerche, IAMC, Oristano, Italy

ARTICLE INFO

Keywords:
DOC
CDOM
FDOM
Oil spill
Polycyclic aromatic hydrocarbons
Fluorescence
Excitation emission matrix
PARAFAC

ABSTRACT

Dissolved organic carbon (DOC), chromophoric and fluorescent dissolved organic matter (CDOM and FDOM, respectively) surface distribution was studied during the Serious Game exercise carried out in the Eastern Ligurian Sea, where an oil spill was localized by using satellite images and models. This paper reports the first DOC, CDOM and FDOM data for this area together with an evaluation of fluorescence as a fast and inexpensive tool for early oil spill detection in marine waters. The samples collected in the oil spill showed a fluorescence intensity markedly higher (~5 fold) than all the other samples. The excitation–emission matrixes, coupled with parallel factor analysis (PARAFAC), allowed for the identification in the FDOM pool of a mixture of polycyclic aromatic hydrocarbons, humic-like and protein-like fluorophores.

1. Introduction

Oil spills represent a serious issue for marine environment. Total anthropogenic input to the marine environments was estimated to account for approximately 112 million tons of oil per year, mainly as a result of oil tanker or pipeline spills (Kvenvolden and Cooper, 2003). This is particularly serious for the Mediterranean Sea, where the annual maritime transport of crude oil and refined products was estimated to be 20% of the total world oil maritime transport (IMO, 1998). The Mediterranean Sea is crossed every year by ~220,000 vessels of more than 100 GRT (Gross Register Tonnage) each discharging approximately 250,000 t of oil due to marine or land-based operations plus further 5000 t per year due to shipping accidents (estimate based on data collected between 1990 and 2005) (EEA, 2006). The oil, spilled into the sea, can be affected by different processes such as: spreading, evaporation, emulsification, photo-oxidation and dispersion. Even if some of these processes immediately affect marine organisms, the negative effects of the oil can persist for a long period (Bianchi et al., 2014; Hong et al., 2015; Zengel et al., 2015). The oil strongly interacts with the largest reservoir of organic molecules dissolved in seawater, the dissolved organic matter (DOM), with a consequent change in oil bioavailability (Ziervogel et al., 2012). Following Deepwater Horizon oil spill (Gulf of Mexico, April 2010), these authors observed a marked change in the rates of heterotrophic carbon degradation and in the turnover of dissolved organic carbon (DOC) in oil contaminated waters. Once these compounds are used by microbes they can be channeled into the food web through the microbial loop.

Polycyclic aromatic hydrocarbons (PAHs) are a component of crude oil that is toxic, mutagenic, and carcinogenic. PAHs are photochemically reactive and have peculiar fluorescence properties, that make them part of both chromophoric DOM (CDOM) and fluorescent DOM (FDOM) (Christensen et al., 2005; Ferretto et al., 2014; Mendoza et al., 2013, D'Sa et al., 2016). CDOM is defined as the fraction of DOM capable of absorbing light at the visible and UV wavelengths, while FDOM is the fraction of CDOM capable of fluorescence. These two fractions can be studied with absorption and fluorescence techniques and allow to gain qualitative information on DOM pool. Fluorescence has been extensively used to study the DOM dynamics, following the Deepwater Horizon Oil Spill (D'Sa et al., 2016; Zhou et al., 2013; Ziervogel et al., 2012). Fluorescence analysis are fast, cheap, easily adaptable to the field, highly sensible and they do not need reagents and extensive sample pretreatments. Excitation emission matrix (EEM) spectroscopy combined with parallel factor (PARAFAC) analysis allows for the identification in the CDOM pool not only of protein-like and humic-like substances, but also of PAH-like compounds. This technique therefore represents a cheap and fast alternative to the classical chemical analysis for the initial discrimination of oil types (Murphy et al., 2008; Ferretto et al., 2014; D'Sa et al., 2016). Only two papers report EEM+PARAFAC for the Mediterranean Sea; one

E-mail address: margherita.gonnelli@pi.ibf.cnr.it (M. Gonnelli).

http://dx.doi.org/10.1016/j.dsr2.2016.05.027
0967-0645/

is focused on the Marseille Bay affected by a municipal sewage effluent (Tedetti et al., 2012); the other one on the Marmara Sea and Dardanelles Straits, in the North Aegean Sea (Zeri et al., 2014).

In the framework of the MEDESS-4MS project, during the Serious Game exercise, water samples were collected in the Eastern Ligurian Sea, in order to study for the first time the surface distribution of DOC, CDOM and FDOM in this area, its variability on the short temporal scale and the use of FDOM as an useful indicator of oil spill also in poorly contaminated marine waters.

2. Materials and methods

2.1. Study area and sampling stations

Two daily cruises were carried out in May 17th 2014 (SG1A) and May 21st 2014 (SG1B) in the Eastern Ligurian Sea, in the area located between the islands of Elba and Capraia and the Italian continental coast (Fig. 1). This area, characterized by a bottom depth of ~200 m, is the main route for commercial vessels between the northern and southern Italy and toward the North Africa and the eastern Mediterranean Sea (data from the Italian Coast Guard, not shown). It was therefore chosen for the experiment due to its high maritime traffic and the consequent high probability of oil spill.

CTD profiles were collected on board the M/V CP406 Antonio Scialoja using a CTD Seabird SBE19 in 45 stations covering the whole study area with a horizontal resolution of ~5.56 km. Data were pre-processed through the SBE software and processed following post-processing QA/QC procedures. Finally, flags were assigned according to visual inspection of data values and scatter/line plots.

Samples for DOC, CDOM and FDOM analysis were collected in 9 stations in both cruises (red dots in Fig. 1). Five additional stations were sampled during:

- SG1A (M1, M2 and M3, black squares in Fig. 1) in the oil spill, localized by satellite images and models (De Dominicis et al., this issue),
- SG1B (D6 and D7, green triangles in Fig. 1) in the area where a small oil spill was identified by satellite, however in-situ visual inspection did not confirmed the presence of the oil.

Samples were collected at the surface (1 m) with a Niskin bottle, they were filtered through a sterile 0.2 μm nylon filter and stored at 4 °C in 200 ml dark glass bottles until the analysis, carried out in 1 week. Bottles were pre-conditioned with filtered deep seawater and rinsed three time with the sample before its collection. Three replicates were collected for each sample. During SG1A, samples in the oil slick (stations M1, M2, M3) were also collected in 3 × 60 ml polycarbonate Nalgene bottles and frozen unfiltered.

Before the analysis, samples were brought to room temperature.

2.2. DOC analysis

DOC measurements were carried out in the shore laboratory with a Shimadzu TOC-Vcsn. Samples were acidified with 2N high purity HCl and sparged for 3 min with CO_2-free ultra-high purity air in order to remove inorganic carbon. From 3 to 5 replicate injections were performed until the analytical precision was lower than 1%. A four-point calibration curve was done with standard solutions of potassium hydrogen phthalate in the same concentration range as the samples. The system blank was measured every day at the beginning and the end of analyses using

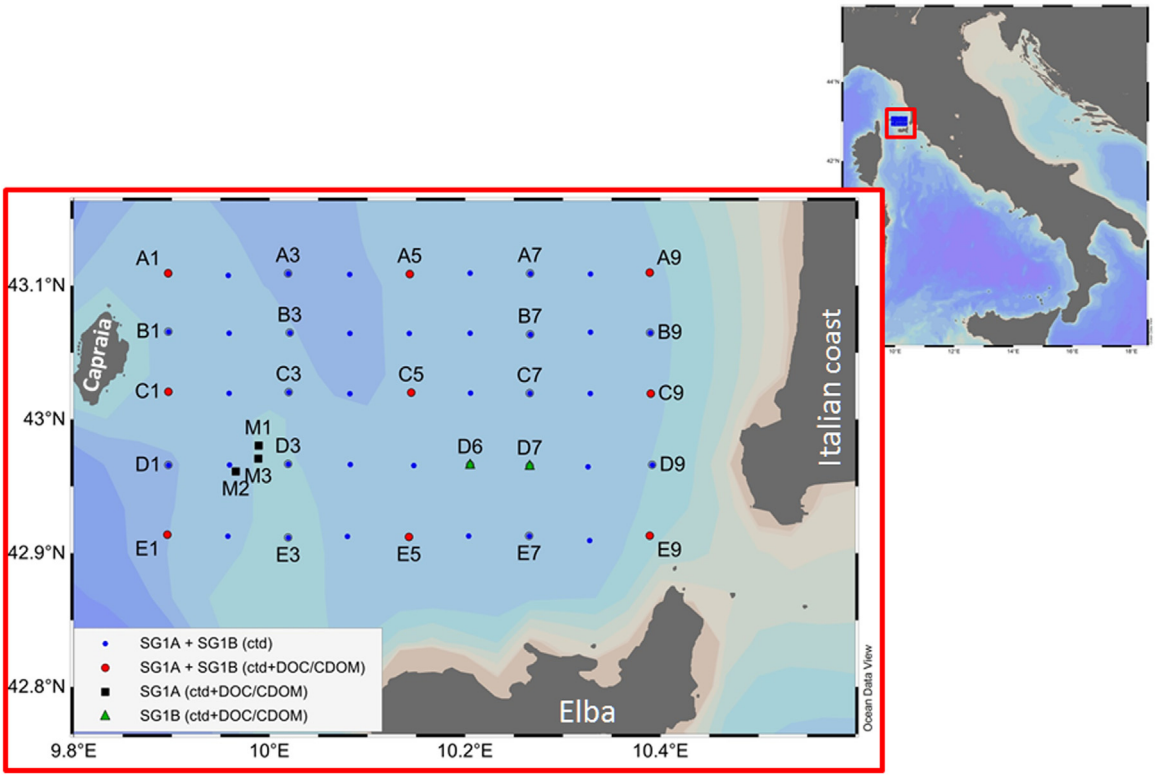

Fig. 1. Study area and sampling stations during the Serious Game exercises, carried out in May 17th (SG1A) and 21st (SG1B) 2014. (For interpretation of the references to color in this legend, the reader is referred to the web version of this article.)

Please cite this article as: Gonnelli, M, et al., Dissolved organic matter dynamics in surface waters affected by oil spill pollution: Results from the Serious Game exercise. Deep-Sea Res. II (2016), http://dx.doi.org/10.1016/j.dsr2.2016.05.027

low-carbon water (2–3 μM C) produced by a Milli-Q system. Measurement reliability was assessed twice a day by comparison of data with DOC Consensus Reference Waters (CRM; Hansell, 2005) (measured concentration = 42.7 μM, nominal concentration: 41–44 μM).

2.3. CDOM optical properties

2.3.1. Absorption

Absorbance spectra were registered between 230 and 700 nm every 0.5 nm, using a Jasco Mod-7850 spectrophotometer with a 10 cm quartz cuvette.

Absorption coefficients (a) were calculated by the Eq. (1):

$$a_{(\lambda)} = 2.303 \cdot A_{(\lambda)}/l \quad (1)$$

where $A_{(\lambda)}$ is the absorbance at wavelength λ and l is the path length expressed in meters. The values were calculated at the following wavelengths: 254, 280, 325, 355 and 443 nm. 280 and 355 nm were chosen because of the maximum in protein-like and humic-like absorption, 254, 325 and 443 were selected in order to facilitate the comparison with the literature.

The dependence of $a_{(\lambda)}$ on λ is typically described by the Eq. (2):

$$a_{(\lambda)} = a_{(\lambda 0)} \cdot e^{-S(\lambda - \lambda 0)} \quad (2)$$

where S is the spectral slope coefficient in the λ–λ_0 nm spectral range. Spectral slope coefficients were estimated using a non-linear fitting over the 275–295 nm spectral range according to Fichot and Benner (2012).

2.3.2. Fluorescence

A FluoroMax4 Horiba-Jobin Ivon Spectrofluorometer (model FP770), with 10 × 10 mm^2 quartz cuvettes, was used to measure single fluorescence emission spectra; the slit-widths were set at 5 nm for both excitation and emission wavelength. This instrument is one of the most sensitive spectrofluorometer, it employs a photon-counting detector for high signal to noise ratio. Due to its high sensitive it is uniquely suited for single spectrum acquisition of samples with low fluorescence intensity. However, the time consuming acquisition makes this instrument not the best choice to measure EEMs.

EEMs were therefore measured using the Aqualog Spectrofluorometer, (Horiba-Jobin Ivon). This instrument has been specifically developed to measures EEMs of FDOM. It is equipped with a TE-cooled CCD fluorescence emission detector allowing for data-acquisition up to 100 times faster than any other benchtop fluorimeter. The fast acquisition also maintains photobleaching at its minimum. The emission spectra were measured in the range 212–619 nm at 3 nm increment over an excitation wavelength ranging between 250 and 450 nm at 5 nm increment.

Both single spectra and EEMs signals were corrected for instrumental bias in excitation and emission and for the inner-filter effect, by using Eq. (3) (Lakowicz, 2006):

$$F_{corr} = F_{obs} 10^{\frac{Abs_{Ex} + Abs_{Em}}{2}} \quad (3)$$

Spectra (and EEMs) were subtracted by the spectrum (and EEM) of Milli-Q water (blank) measured before each sample in the same conditions as the sample.

In the EEMs, Rayleigh and Raman scatter peaks were removed by using the monotone cubic interpolation (shape-preserving) (Carlson and Fritsch, 1989), since blank subtraction did not completely removed their signals.

Spectra were normalized to the water Raman signal, dividing the fluorescence by the integrated Raman band of Milli-Q water (λ_{ex} = 350 nm, λ_{em} = 371–428 nm), measured the same day of the analysis with the two instruments. The fluorescence intensity is therefore reported as equivalent water Raman Units (R.U.) (Lawaetz and Stedmon, 2009).

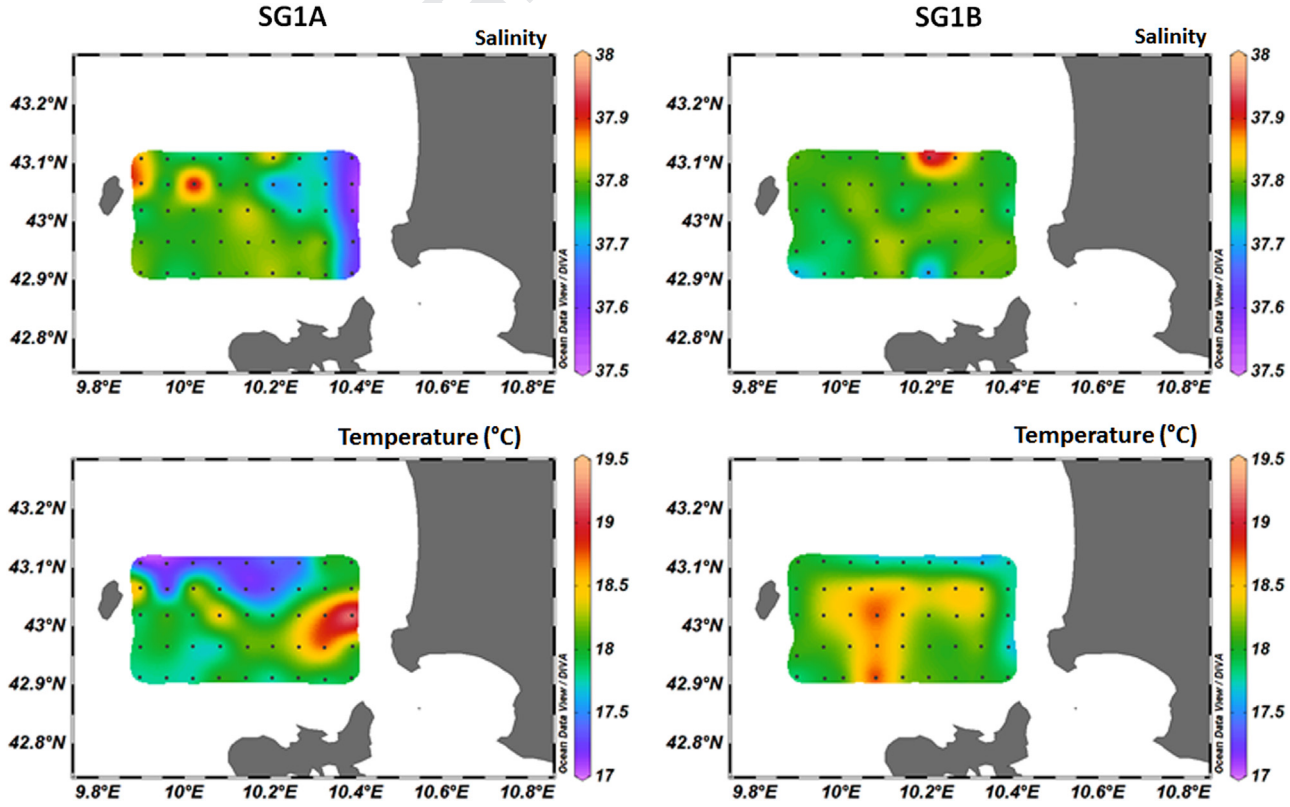

Fig. 2. Surface distribution of salinity and temperature in the two cruises. The black points refer to the data used for the interpolation.

Please cite this article as: Gonnelli, M, et al., Dissolved organic matter dynamics in surface waters affected by oil spill pollution: Results from the Serious Game exercise. Deep-Sea Res. II (2016), http://dx.doi.org/10.1016/j.dsr2.2016.05.027

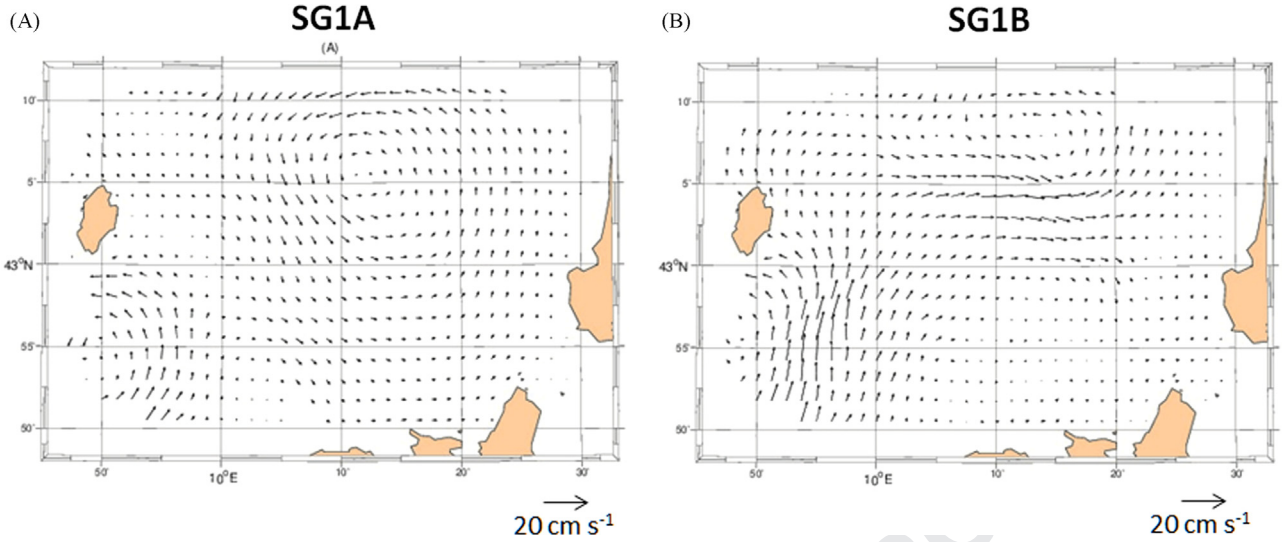

Fig. 3. Steady state circulation, computed from diagnostic calculations for the two cruises carried out in (a) May 17th and (b) May 21st.

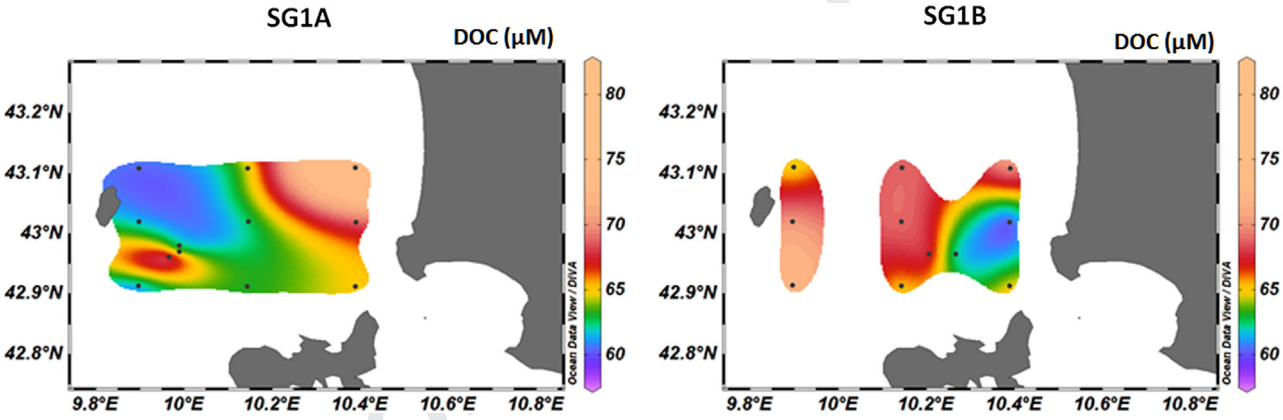

Fig. 4. Surface distribution of DOC in the two cruises. The black points refer to the data used for the interpolation.

2.3.3. *PARAFAC modeling*

The parallel factorial analysis (PARAFAC) (DOM Fluor Toolbox, Stedmon and Bro, 2008) was applied to the 72 EEMs collected during the two cruises. EEMs were normalized to their maximum before to run PARAFAC, in order to avoid the removal of the high intensity EEMs (e.g. the one measured at stations M2 and M3) as outliers. A 4-component model was validated. The fluorescence intensity of the 4 components for every sample was calculated multiplying the output of the PARAFAC modeling by the factor of normalization previously applied.

2.4. *Data elaboration*

Horizontal maps were made using the latest Ocean Data View Version: ODV 4.7.4. (Schlitzer, R., Ocean Data View, odv.awi.de, 2015). The spectra were elaborated by using OriginPro9.

3. Results and discussion

3.1. *Physical data*

Different physical conditions were observed in the two cruises (Fig. 2), even if they were carried out very close in time (3 days). During SG1A, salinity showed low values (<37.65) in the stations close to the coast, with a minimum ($S<37.60$) at stations A9, B9 and C9. The low salinity of this surface water suggests that it is probably mixed with continental waters. Temperature surface map shows a clear front separating cold ($T<17.6$ °C) water at the northern stations from warmer waters ($T>18$ °C) at the southern stations (Fig. 2). The steady state circulation, computed from diagnostic calculations, showed the occurrence of a cyclonic eddy located between Capraia island and the coast of Tuscany (Fig. 3a). The diameter of this structure is ~50 km, it can be therefore ascribed as a small mesoscale feature. It largely dominates the surface circulation of the study domain with a maximum speed of ~10 cm s^{-1} along the thermal front. The cyclonic rotation leads to the spreading of the sea surface waters mass from the center (divergence) and to the upwelling of deeper and colder water (17.15 °C) coming from the thermocline at approximately 40 m depth. A second cyclonic eddy was observed between Capraia and Elba islands at the south-western limit of the sampling area. A more detailed description of the steady circulation, derived from numerical modeling, is reported in Sorgente et al. (this issue).

During SG1B surface distribution of both salinity and temperature shows a completely different pattern with respect to SG1A due to the turbulent mixing induced at the surface by wind and coastal currents advection. During both cruises, the wind

Please cite this article as: Gonnelli, M, et al., Dissolved organic matter dynamics in surface waters affected by oil spill pollution: Results from the Serious Game exercise. Deep-Sea Res. II (2016), http://dx.doi.org/10.1016/j.dsr2.2016.05.027

Table 1
DOC, CDOM and FDOM values for the samples collected during the two surveys (SG1A, May 17th and SG1B, May 21st).

Station	Cruise	DOC [μM]	$S_{275-295}$ [nm^{-1}]	$S_{350-400}$ [nm^{-1}]	a_{254} [m^{-1}]	a_{280} [m^{-1}]	a_{325} [m^{-1}]	a_{355} [m^{-1}]	a_{443} [m^{-1}]	C1 [R.U]	C2 [R.U]	C3 [R.U]	C4 [R.U]	C1/C3
A1	SG1A	60.4	0.0378	0.0155	1.359	0.669	0.163	0.081	0.014	0.015	0.015	0.006	0.007	2.298
	SG1B	64.9	0.0374	0.0209	1.423	0.704	0.149	0.074	0.013	0.014	0.013	0.005	0.007	2.640
A5	SG1A	64.5	0.0378	0.0199	1.365	0.667	0.147	0.077	0.010	0.014	0.013	0.005	0.006	2.639
	SG1B	69.0	0.0373	0.0208	1.402	0.699	0.162	0.079	0.013	0.013	0.015	0.004	0.007	3.091
A9	SG1A	81.9	0.0348	0.0193	1.655	0.952	0.225	0.127	0.030	0.029	0.025	0.011	0.012	2.513
	SG1B	70.0	0.0380	0.0231	1.383	0.686	0.144	0.069	0.012	0.014	0.012	0.005	0.007	2.882
C1	SG1A	61.6	0.0383	0.0231	1.375	0.695	0.151	0.068	0.005	0.013	0.017	0.007	0.007	1.860
	SG1B	70.3	0.0366	0.0215	1.382	0.685	0.153	0.079	0.015	0.013	0.014	0.005	0.006	2.820
C5	SG1A	62.6	0.0378	0.0155	1.372	0.695	0.150	0.087	0.010	0.014	0.015	0.006	0.007	2.316
	SG1B	69.0	0.0385	0.0235	1.353	0.675	0.152	0.081	0.011	0.016	0.014	0.004	0.007	3.600
C9	SG1A	68.9	0.0328	0.0233	1.689	0.930	0.269	0.129	0.016	0.024	0.025	0.009	0.018	2.585
	SG1B	60.3	0.0383	0.0214	1.382	0.690	0.140	0.079	0.011	0.013	0.015	0.005	0.006	2.414
E1	SG1A	61.8	0.0371	0.0180	1.440	0.729	0.174	0.089	0.017	0.018	0.012	0.006	0.008	2.975
	SG1B	73.5	0.0389	0.0151	1.471	0.820	0.163	0.091	0.028	0.015	0.015	0.005	0.007	2.973
E5	SG1A	63.2	0.0344	0.0135	1.370	0.710	0.166	0.091	0.017	0.014	0.016	0.007	0.008	2.082
	SG1B	65.5	0.0403	0.0312	1.344	0.653	0.142	0.063	0.003	0.013	0.012	0.004	0.006	3.080
E9	SG1A	64.9	0.0368	0.0197	1.577	0.938	0.210	0.101	0.019	0.019	0.019	0.008	0.010	2.228
	SG1B	64.5	0.0395	0.0287	1.380	0.687	0.143	0.053	0.010	0.014	0.012	0.004	0.006	3.547
M1	SG1A	62.6	0.0294	0.0132	1.690	0.971	0.287	0.178	0.050	0.020	0.014	0.007	0.008	2.860
M2	SG1A	68.0	0.0297	0.0167	1.854	1.044	0.330	0.192	0.052	0.071	0.021	0.003	0.010	20.941
M3	SG1A	63.6	0.0351	0.0159	1.525	0.805	0.215	0.123	0.035	0.015	0.020	0.007	0.011	2.015
D6	SG1B	67.5	0.0353	0.0234	1.389	0.749	0.150	0.079	0.012	0.023	0.014	0.005	0.008	4.472
D7	SG1B	62.4	0.0392	0.0247	1.250	0.615	0.118	0.062	0.001	0.018	0.014	0.006	0.008	3.252

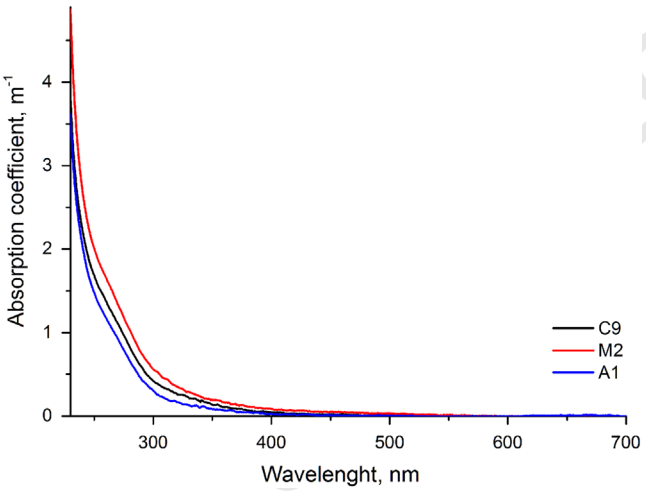

Fig. 5. Example of absorption spectra measured during SG1A at 3 stations representative of the diversity of the study area.

speed was low, but in between them, strong southern winds blew and this can explain the marked change in surface circulation observed in only 3 days. The salinity minimum ($S \approx 37.7$) was visible only at stations E1 and E6 while its maximum was observed at station A6. Waters with a temperature lower than 17.7 °C occurred at 2 northern stations (A7 and A8). High temperature (> 18.4 °C) characterized the central part of study area with a maximum ($T > 18.6$ °C) at stations E4, D4, C4. Modeled circulation shows a salt front located along the northern boundary of the study area; this front is also visible in temperature distribution (Fig. 2) and is associated with the convergence at the surface of saltier and colder water masses coming from the depth and induced by the first cyclonic eddy previously described. This feature, which now moved north-eastward, was partially detected by the model on the northern open boundary, in favor of the anticyclonic eddy lee of the Elba island. Such an eddy reversed the circulation along the northern Elba isobath of about 100 m from eastward during SG1A to westward during SG1B.

3.2. Dissolved organic carbon (DOC)

DOC concentration ranged between 62 and 82 μM in SG1A and between 60 and 73 μM in SG1B (Fig. 4 and Table 1). This is the range usually observed in surface waters, both in the ocean (Lønborg and Álvarez-Salgado, 2014; Hansell, 2013) and in the Mediterranean Sea (Santinelli, 2015). Though the two cruises were carried out very close in time (May 17th and 21st), DOC distribution changed, in agreement with the change in circulation pattern. The highest value (82 μM) was observed during SG1A close to the coast, at the stations A9 and C9, in correspondence to the minimum in salinity (Fig. 4). This maximum can be therefore explained by the occurrence of a vein of water impacted by terrestrial inputs, coming from the south. It is also noteworthy the increase in DOC concentration in the area interested by the oil slick during SG1A (station M2). Here DOC was 6 μM higher than in the close stations C1, C5, E1 and E5 (68 μM vs. 62 μM).

During SG1B, the DOC distribution showed a good agreement with the circulation pattern described above. The DOC maximum was observed at the station E1 (Fig. 4), where a slight decrease in salinity was also observed (Fig. 2). High DOC concentrations characterized the northward current visible in the surface circulation (Fig. 3). These data stress the strong influence of surface currents in shaping DOC distribution, in particular in areas close to the coast and impacted by terrestrial input.

3.3. Absorption

Three CDOM absorption spectra, measured during SG1A, are reported in Fig. 5, as an example. These stations were chosen as representative of the diversity of the study area: station C9 is close

Please cite this article as: Gonnelli, M, et al., Dissolved organic matter dynamics in surface waters affected by oil spill pollution: Results from the Serious Game exercise. Deep-Sea Res. II (2016), http://dx.doi.org/10.1016/j.dsr2.2016.05.027

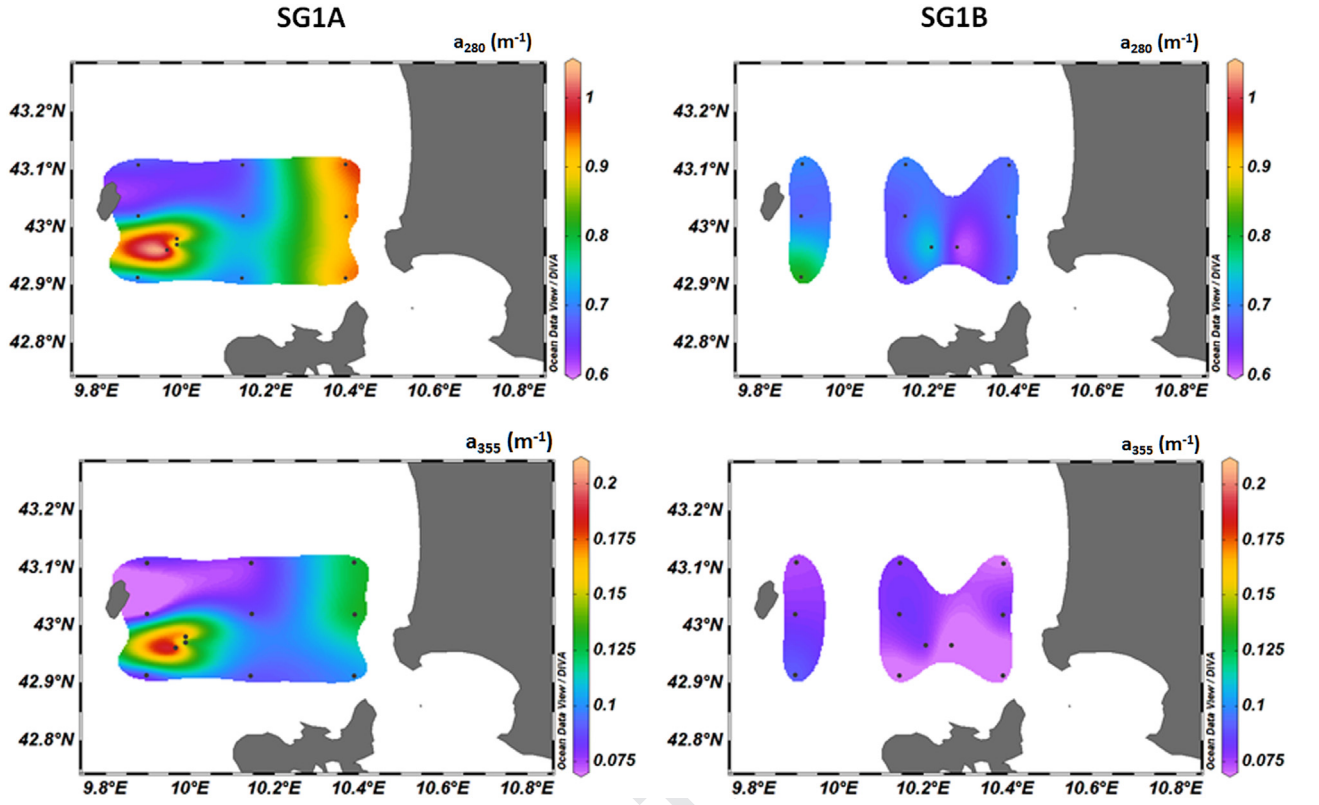

Fig. 6. Surface distribution of absorption coefficient at 280 and 355 nm. The black points refer to the data used for the interpolation.

to the coast and characterized by a minimum of salinity and a maximum of temperature, station M2 is located in the oil slick and station A1 is the station farthest from the coast and characterized by a maximum of salinity and a minimum of temperature. The 3 spectra show the classical unstructured shape with the near-exponential decrease at increasing wavelengths (from the ultra-violet to the visible region). The CDOM absorption at station M2 (oil slick) was higher than in the other 2 stations, in particular in the UV region (Fig. 5, Table 1). This observation confirms the occurrence in CDOM pool of tracers of oil spill pollution such as aniline derivatives, polyenes and polycyclic aromatic hydrocarbons with two or more aromatic rings (Chin et al., 1994; Peuravuori and Pihlaja, 1997).

The values of absorption coefficient at 5 representative wavelengths were calculated in order to study CDOM concentration and dynamics in the study area as well as to make a comparison with the literature (Table 1). Absorption coefficient at 254, 325 and 340 nm (a_{254}, a_{325}, a_{340}), are widely used in the literature as indicator of CDOM concentration (Stedmon and Nelson, 2015; Liu et al., 2014; Kowalczuk et al., 2003); while the absorption coefficient at 280 and 355 nm (a_{280}, a_{355}) are characteristic of protein-like and humic-like substances, respectively (Seritti et al., 1998). a_{254} ranged between 1.34 and 1.85 m^{-1} (Table 1), these values are similar to those reported for the eastern boundary of the temperate North Atlantic in July–August 2009 (1.2–1.8 m^{-1}) (Lønborg and Álvarez-Salgado, 2014). a_{340} ranged between 0.09 and 0.24 m^{-1} (Table 1), these values are slightly higher than those reported for surface waters of the Atlantic, Pacific and Indian oceans (0–0.17 m^{-1}), in particular for the subtropical gyres, where very low values were observed (0–0.03 m^{-1}) (Stedmon and Nelson, 2015). a_{355} ranged between 0.07 and 0.19 m^{-1} (Table 1 and Fig. 4), these values are in the same range of those found offshore (a_{350}=0.07–0.13 m^{-1}) the Rhone Estuary (SOFCOM

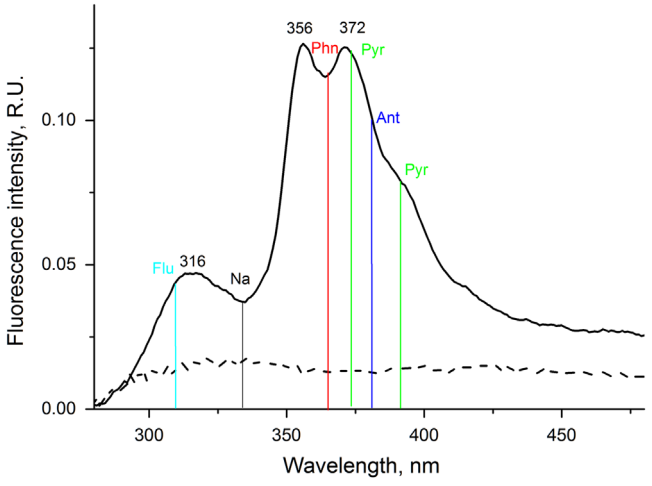

Fig. 7. Single fluorescence spectra excited at 255 nm of filtered samples collected at station M2 (continuum line) and at station M1 (dotted line). The six vertical line refer to the emission peaks of the principal components of oil. Flu: fluorene; Na: naphthalene; Phn: phenanthrene; Pyr: pyrene; Ant: anthracene.

station) in 2007 and 2008 (Para et al., 2010), while they are higher than those reported for the surface sample collected at BATS (0.05–0.09 m^{-1}) (Nelson et al., 1998) and lower than those collected in both the North Sea (0.16–1.51 m^{-1}) (Stedmon et al., 2000) and in the Onslow Bay (0.06–0.98 m^{-1}) (Kowalczuk et al., 2003). Finally, both a_{280} and a_{355} (0.61–1.04 and 0.05–0.19 m^{-1}) showed values lower than those observed in the Northern Adriatic Sea, close to the Po river mouth in 2003 and 2004, (average of a_{280}: 1.6–2.2 m^{-1}, of a_{355}: 0.3–0.5 m^{-1}) (Berto et al., 2010), in coastal water of the Tyrrhenian Sea affected by Arno river input and

Please cite this article as: Gonnelli, M, et al., Dissolved organic matter dynamics in surface waters affected by oil spill pollution: Results from the Serious Game exercise. Deep-Sea Res. II (2016), http://dx.doi.org/10.1016/j.dsr2.2016.05.027

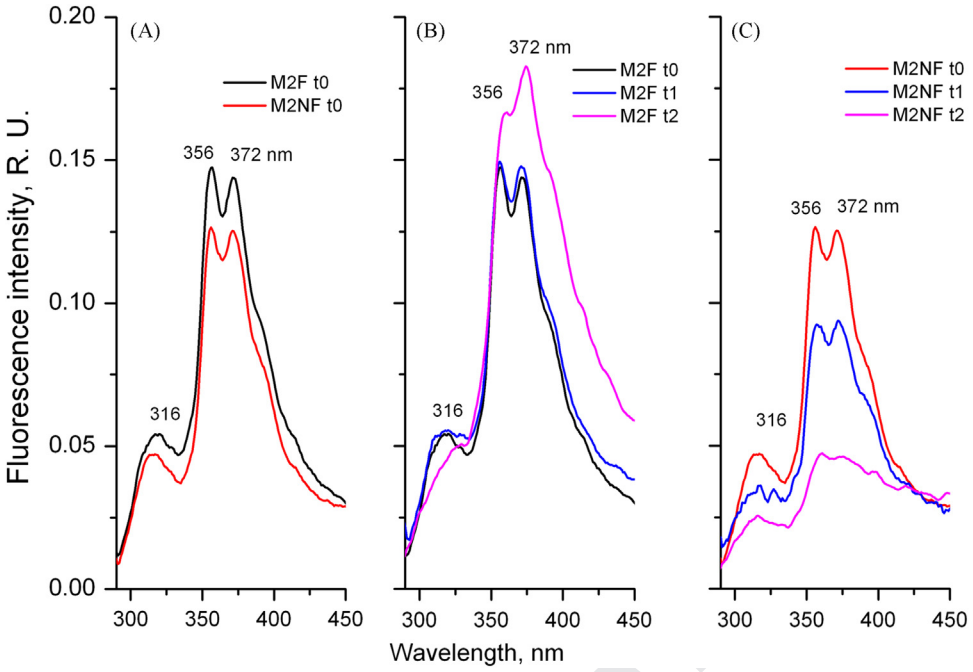

Fig. 8. Comparison of fluorescence spectrum for filtered (stored at 4 °C) and unfiltered (stored at −20 °C) samples (A). Change with time of the fluorescence spectra of filtered (B) and unfiltered (C) samples collected at station M2. t0: time zero; t1: after 24 h at 22 °C; t2: after 1 month at 4 °C. The numbers refer to the wavelength of the emission peaks.

Livorno harbor in September 1997 (a_{280}: 0.95–2.3 m^{-1}; a_{355}: 0.14–0.57 m^{-1}) (Seritti et al., 1998) and in offshore water in front of Arno river mouth (a_{280}: 1.26–1.29 m^{-1}; a_{355}: 0.3 m^{-1}) (Gonnelli et al., 2013; Retelletti Brogi et al., 2015).

These results suggest that surface DOM concentration in the study area was similar to that of open ocean areas excluding the subtropical gyres, where the high photobleaching strongly reduced CDOM absorbance, but it was lower than in coastal waters impacted by river inputs.

Very similar surface distribution was observed for a_{280} and a_{254} as well as a_{355}, a_{325} and a_{443}. The surface map of a_{280} and a_{355} is therefore reported as representative of the dynamics of CDOM in the surface layer during the two cruises. Both a_{280} and a_{355} showed a complex pattern and a marked variability between the two cruises (Fig. 6), in agreement with DOC distribution (Fig. 4). During SG1A, absorption showed the highest value, at all the wavelengths, in the oil spill (station M2) (Fig. 6 and Table 1). High values were also observed in the stations close to the coast (A9, E9 and C9), in correspondence with the highest DOC values and the minimum in salinity (Figs. 2 and 4). The increase near the shore could be explained by the occurrence of continental waters, probably affected by the Cornia river flowing in the Follonica Gulf, as suggested by the low salinity and high DOC concentration (Fig. 4). It is noteworthy that absorption values in the oil slick were up to 1.6, 2.1 and 3.3 time higher than those at the stations close to the coast (average between A9 and C9) for a_{325}, a_{355} and a_{443}, respectively.

During SG1B, values of both a_{280} and a_{355} were markedly lower than those observed during SG1A, without noticeable increase close to the coast. a_{280} showed a slight increase (0.82 m^{-1}) at station D6 in correspondence to a slightly less salty waters. The decrease of absorption in the stations close to the coast is in agreement with DOC pattern and can be easily explained by the change in surface circulation, that prevented the less salty waters, mixed with continental waters, to remain close to the coast.

The spectral slope in the range 275–295 nm ($S_{275-295}$) was calculated in order to gain information about the molecular characteristics of CDOM (Table 1). $S_{275-295}$ has been considered an useful biogeochemical indicator. An increase in its value has been attributed to a decrease in molecular weight and aromaticity degree of CDOM (Helms et al., 2008). $S_{275-295}$ ranged between 0.029 and 0.040 nm^{-1}. Values higher than 0.03 nm^{-1} are usually observed in open sea waters, while values lower than 0.03 nm^{-1} indicates the occurrence of molecules with high molecular weight and aromaticity degree, that usually come from the rivers (Fichot and Benner, 2012). These data suggest that most of CDOM is marine, however it is noteworthy the minimum of $S_{275-295}$ (0.029 nm^{-1}) was observed in the oil spill (stations M1 and M2), suggesting an increase in the aromaticity degree typical of PAHs compounds (Table 1). As for absorption, during SG1B the values of $S_{275-295}$ were higher and more homogeneous than those observed during SG1A, with values ranging between 0.035 and 0.040 nm^{-1} (Table 1).

Synthetizing, these data highlight that surface circulation as well as the oil spill affect optical properties of the surface waters and that absorption can be a good tracer not only of terrestrial input but also of oil contamination.

3.4. Fluorescence

3.4.1. Single fluorescence emission spectra in the oil spill (stations M1 and M2)

Single emission spectra of the samples collected in the oil spill were measured at stations M1 and M2 using the excitation wavelengths usually used in PAHs sensors (λ_{ex}=255 nm). Station M2 was the most affected by the oil spill, as indicated by the results of the model (De Dominicis et al., this issue). The average

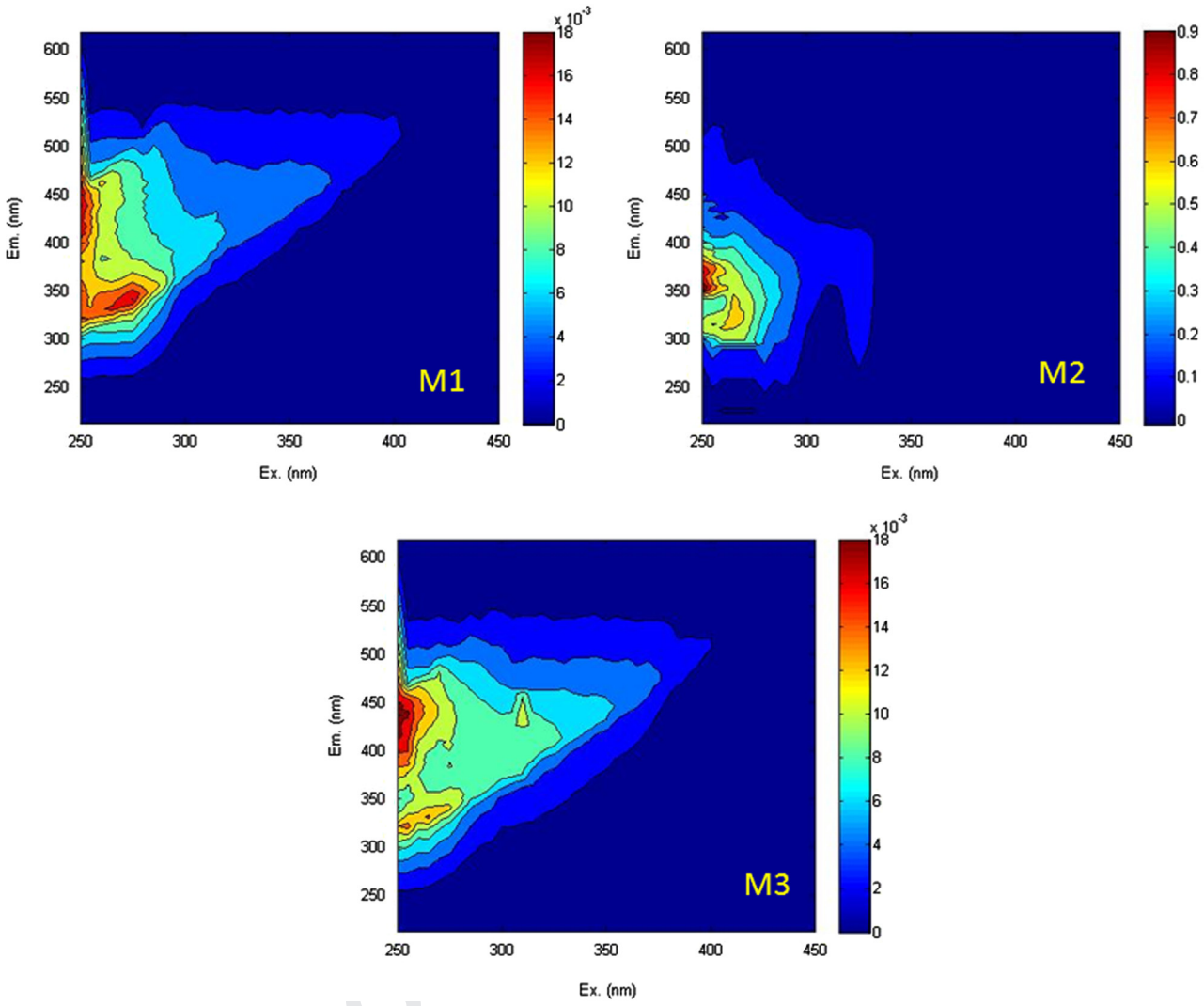

Fig. 9. Excitation Emission Matrixes (EEMs) of the stations located in the oil spill: M1, M2 and M3.

fluorescence emission spectrum of the filtered samples collected at station M2 was characterized by a well resolved shape, with 3 defined peaks, that are not usually observed in open sea waters, and an intensity 5-times higher than the spectra of the samples collected in the closest stations (C1, C5, E1, E5) (Fig. 7). This signal was not observed in the samples collected at station M1 (Fig. 7, dotted line). Even if three peaks (λ_{em}=316 nm, 356 nm and 372 nm) can be identified, this spectrum is broader than the classic spectrum due to a single component and it does not match with any other spectrum of the known compounds present in the oil, it therefore could indicate the occurrence of a complex mixtures of PAHs. The comparison of the observed peaks with those due to the principal oil components (vertical line in Fig. 7) suggests that the first peak could be due to fluorene and the other two to a mixture of phenantrene, pyrene and anthracene-like compounds, even if the occurrence of other PAHs with unknown fluorescence signatures cannot be excluded.

3.4.2. *Storage conditions for PAHs analysis*

Samples for PAHs determination are usually stored unfiltered at 4 °C (Ramirez et al., 2014; Ramos-Dorta et al., 2013; ARPAT protocols). The samples, collected during SG1A in the oil spill, were filtered through a 0.2 μm nylon filter and stored at 4 °C, as the other samples. However, due to the sticky properties of oil, filtration would potentially cause an underestimation of PAHs, so 3 additional samples were stored unfiltered at −20 °C, in order to avoid any chemical (filtration) and biological (microbial removal) alteration of the sample. All the samples were brought at room temperature before the analysis. The comparison among filtered and unfiltered samples allows for a check of possible oil removal by filtration (Fig. 8a). Both the treatments (3 filtered and 3 unfiltered replicates) were re-analyzed after 24 h (t1), stored at room temperature (~22 °C), and after 1 month, stored at 4 °C (t2) (Fig. 8b and c), in order to check for possible microbial removal of the oil in the unfiltered samples.

The fluorescence spectra of filtered (stored at 4 °C) and unfiltered (stored at −20 °C) samples showed the same shape with 3 well defined peaks, however a slight decrease (~13%) can be observed in the sample stored at −20 °C, suggesting that filtration does not remove PAHs while freezing could determine their undersetimation (Fig. 8a). It is noteworthy that after 24 h at room temperature, fluorescence intensity showed 33% decrease in the unfiltered samples but no change in the filtered sample. After 1 month at 4 °C, the difference in fluoresce intensity between filtered and unfiltered samples was even more marked with 85%

Please cite this article as: Gonnelli, M, et al., Dissolved organic matter dynamics in surface waters affected by oil spill pollution: Results from the Serious Game exercise. Deep-Sea Res. II (2016), http://dx.doi.org/10.1016/j.dsr2.2016.05.027

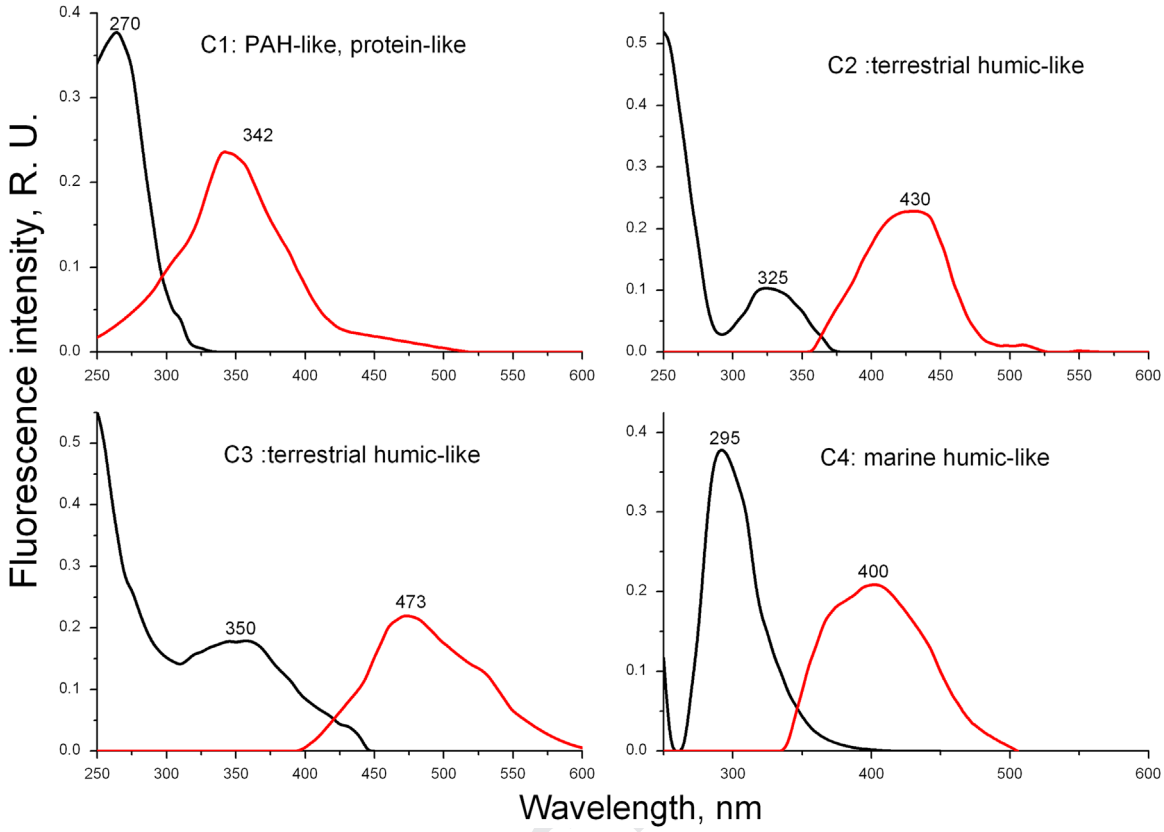

Fig. 10. Excitation (black line) and emission (red line) spectra of the four components obtained by fluorescence PARAFAC modeling. (For interpretation of the references to color in this figure legend, the reader is referred to the web version of this article.)

decrease in unfiltered samples and a slight increase together with a red shift of the 3 peaks in filtered samples (Fig. 8b and c).

It is interesting to notice that in the unfiltered samples collected in the slick, DOC concentration quickly decreased, up to 62 μM after 1 month at 4 °C, indicating the fast removal of oil by microbes, while in the filtered samples (0.2 μm), where bacterial were removed, the DOC concentration did not decrease. These results support that indigenous marine microorganisms have the metabolic pathways to quickly degrade oil (Das and Chandran, 2010). These toxic compounds can be therefore channeled into the food web through the microbial loop. The removal of the oil in the unfiltered samples kept at 4 °C also highlights the importance of a correct storage of the samples for PAHs analysis. The method actually employed by the Agency for Environmental Protection probably leads to an underestimation of the PAHs occurring in seawater.

3.4.3. *Fluorescence excitation emission matrixes in the oil spill*

The comparison of the EEMs, measured at the three stations, located in the oil spill (M1, M2 and M3), confirms that station M2 was the most contaminated by PAHs, with ~5-fold higher fluorescence intensity than all the other samples and 2 well-defined peaks at excitation (λ_{ex})/emission wavelengths (λ_{em}) of 250–270/350–400 nm and 270–280/300–340 nm (Fig. 9). The EEMs, measured at station M1 and M3, showed the classical shape of natural FDOM, with two main peaks, the first one at λ_{ex}=250–270/330–350 nm and λ_{em}=400–450 nm, attributed to humic-like fluorophores; the second one at λ_{ex}=260–290 nm and λ_{em}=330–350 nm, attributed to protein-like fluorophores. These 2 peaks were masked by the oil signal in the EEM measured at station M2.

3.4.4. *Identification of CDOM components*

The PARAFAC analysis applied to the 72 EEMs measured in this study, allowed for the validation of a 4-component model (Fig. 10). The four groups of fluorophores, hereinafter components (C), were identified by comparison with the two papers reporting EEM+PARAFAC for the Mediterranean Sea and the literature for both coastal areas and open ocean (Table 2). C1 shows the excitation peak at 270 nm and the emission maximum at 342 nm, these spectroscopic characteristics have been usually considered typical of protein-like substances in open ocean waters (Coble, 1996; Stedmon and Markager, 2005; Murphy et al., 2008; Kowalczuk et al., 2009; Jorgensen et al., 2011; Tedetti et al., 2012). Recent studies suggest that they are also similar to those of PAHs oil-related, naphthalene-like and phenantrene-like, identified in the Gulf of Mexico post the Deepwater Horizon Oil Spill, in April 2012 and 2013 (G5, D'Sa et al., 2016) as well as to naphthalene and phenantrene individuated by Ferretto et al., 2014. This component can be therefore identified as a mixture of different PAHs and aromatic amino acids (tryptophan and tyrosine).

C2 and C3 were identified as humic-like substances, due to their excitation/emission maximum (C2: λ_{ex}=325 nm, λ_{em}=430 nm; C3: λ_{ex}=350 nm, λ_{em}=473 nm). Both components show spectroscopic characteristics similar to peak A and C observed in the literature and usually found in coastal regions impacted by terrestrial input, they are therefore identified as humic-like FDOM with terrestrial origin (Coble, 1996; Stedmon and Markager, 2005;

Please cite this article as: Gonnelli, M, et al., Dissolved organic matter dynamics in surface waters affected by oil spill pollution: Results from the Serious Game exercise. Deep-Sea Res. II (2016), http://dx.doi.org/10.1016/j.dsr2.2016.05.027

Table 2
Spectroscopic characteristics of the four PARAFAC components validated in this study and their possible identification by comparison with similar components reported in the literature.

Component	Ex/Em	Description
1	270/342	***PAHs-like substances***
		G5, D'Sa et al. (2016);
		Napthalene & Phenantrene, Ferretto et al. (2014)
		Protein-like substances
		Peak T, Coble (1996)
		C7 Stedmon and Markager (2005)
		P7, Murphy et al. (2008)
		C6, Kowalczuk et al. (2009)
		C2, Jorgensen et al. (2011)
		C2, Tedetti et al. (2012)
2	(250)324/430	***Terrestrial humic-like substances***
		Peak A Coble (1996)
		C5, Stedmon and Markager (2005)
		P8, Murphy et al. (2008)
		C2, Kowalczuk et al. (2009)
		C1, Jorgensen et al. (2011)
		C1, Zeri et al. (2014)
		G1, D'sa et al. (2016)
3	350/473	***Terrestrial humic-like substances***
		Peak C, Coble (1996)
		C4, Kowalczuk et al. (2009)
		C5, Tedetti et al. (2012)
		G2, D'Sa et al. (2016)
4	295/400	***Marine humic-like substances***
		Peak M, Coble (1996)
		C6 Stedmon and Markager (2005)
		P1, Murphy et al. (2008)
		C3, Kowalczuk et al. (2009)
		C4, Jorgensen et al. (2011)
		C3, Tedetti et al. (2012)
		G3, D'Sa et al. (2016)

Murphy et al., 2008; Kowalczuk et al., 2009; Zeri et al., 2014). C2 is also very similar to the terrestrial humic-like component found in the open ocean (Jorgensen et al., 2011). C3 is characterized by the highest $\lambda_{ex}/\lambda_{em}$ wavelengths of all the components, it is therefore representative of fluorophores with an higher molecular weight and aromaticity degree, typical of terrestrial CDOM. C3 is also very similar to the humic-like FDOM, observed in the shelf of Gulf of Mexico before the oil spill (G2, D'Sa et al., 2016) as well as to the terrestrial humic-like component identified in Bay of Marseilles (Tedetti et al., 2012). This component was not found in the open oceans (Jorgensen et al., 2011).

The spectroscopic characteristics of C4 (λ_{ex}=295 nm, λ_{em}=400 nm) are similar to those of marine humic-like substances, e.g. peak M according to Coble (Coble, 1996; Stedmon and Markager, 2005; Murphy et al., 2008; Kowalczuk et al., 2009; Tedetti et al., 2012; D'Sa et al., 2016). A similar component, but with the excitation wavelength at 325 nm, was also observed in the open ocean (Jorgensen et al., 2011).

3.4.5. *Surface distribution of CDOM components*

The main feature emerging in the surface distribution of FDOM is the marked variability between the two cruises. Fluorescence was markedly higher and with noticeable differences among stations during SG1A than SG1B (Figs. 11 and 12 and Table 1).

During SG1A, at station M2 (located in the oil spill), C1 component (PAH-like), representative of oil contamination, showed a value (0.07 R.U.), about 5 times higher than in all the other stations ($<$0.03 R.U.) (Fig. 11 and Table 1). This station is also characterized by a marked increase in fluorescence intensity of both "terrestrial" (C2) and "marine" (C4) humic-like components and a minimum of C3 (Figs. 11 and 12). All the humic-like components showed an increase in the stations close to the coast (A9, C9 and E9), in particular the distribution of C2 was remarkably similar to that of DOC (Fig. 4) and a_{355} (Fig. 6). The fluorescence increase in the stations close to the coast occurs also in C1 (Table 1), but it is masked by the occurrence of PAHs at M2 (Fig. 11). C3 and C2 showed their maximum at station A9, in correspondence with the maximum of a_{280}. C4 shows its maximum at station C9, in correspondence with the maximum of temperature.

Fluorescence indices have been used to characterize natural organic matter since 1990s (Gabor et al., 2014). As an example, Baker (2001) proposed to use the ratio between tryptophan-like peak and fulvic-like peak to identified sewage impact on rivers. Here we propose a similar index that can highlight the occurrence of PAHs by dividing the PAH-like component (C1) by C3, that has the spectroscopic characteristics typical of the terrestrial humic-like acid. This index allows to normalize the signal of PAH (C1) to the "terrestrial FDOM" (C3), highlighting the PAH contribution to FDOM pool. The values of the index clearly evidence the oil contamination at station M2, where the index is 6–12 times higher than in the other stations (Table 1).

During SG1B, fluorescence showed values similar to the lowest ones observed in SG1A and differences among stations were very small (Figs. 11 and 12, Table 1), suggesting a general homogeneity of FDOM distribution. A slight increase was observed in C1, C2 and C4 at stations D6 and D7, in correspondence with slightly higher a_{280} values.

These data highlight that FDOM can be a good tracer of oil spill contamination even when the spill is not very large. The combination of the different components highlight the occurrence of continental waters with a much higher sensibility than DOC and absorption. Finally, the marked difference in surface distribution of FDOM between the two cruises clearly indicates that surface circulation is the main driver of FDOM surface distribution.

4. Conclusions

The analysis of CTD data and diagnostic model results, related to the two high resolution surveys carried out in May 17th and 21st 2014 in the Eastern Ligurian Sea, reveal circulation patterns dominated by Ekman currents and not-stationary, small and superficial mesoscale features as cyclonic and anti-cyclonic eddies induced by fluctuating winds at the sea surface. The spatial and temporal variations of the wind speed induce divergent and convergent surface currents, as well as marked change of the coastal currents.

In this context, the first biogeochemical (DOC, CDOM and FDOM) data for this area showed a remarkable change in their surface distribution between the two surveys with a decrease in both absorption and fluorescence values from May 17th to 21st. High values of DOC, CDOM and FDOM were observed in the stations affected by terrestrial input and the oil spill in May 17th. These data suggest that CDOM and FDOM are good tracers of continental water masses and stress that the study of biogeochemical processes must take into account the pattern of surface circulation. The use of EEMs combined with PARAFAC allows for an early detection of oil also in poorly contaminated marine waters. These data further confirm that fluorescence and absorption are fast, cheap and highly sensitive tools to trace oil contamination and they can give a quick and general overview of the area interested by oil spill. FDOM could therefore be a very powerful parameter for tracing the dispersion and evolution of the oil spill in the surface ocean.

Please cite this article as: Gonnelli, M, et al., Dissolved organic matter dynamics in surface waters affected by oil spill pollution: Results from the Serious Game exercise. Deep-Sea Res. II (2016), http://dx.doi.org/10.1016/j.dsr2.2016.05.027

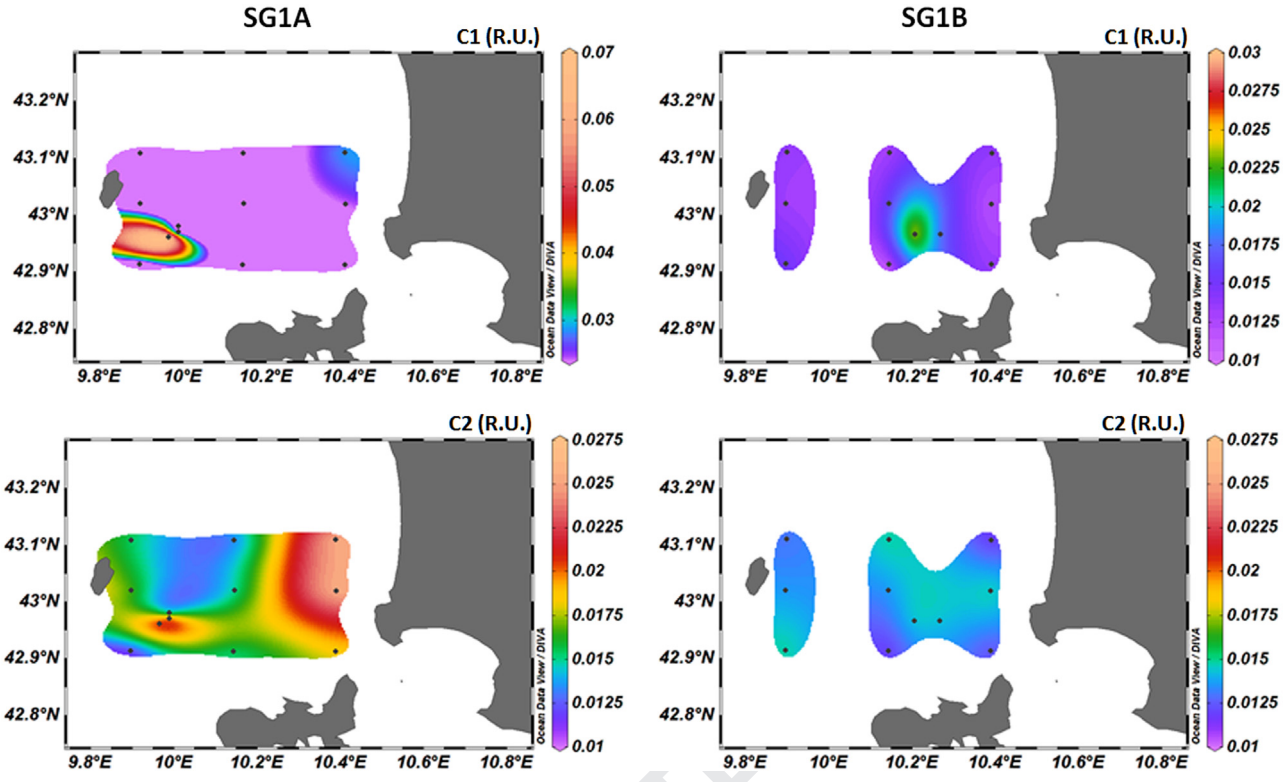

Fig. 11. Surface distributions of PAH-like + protein-like (C1) and humic-like (C2) components in the two cruises. The black points refer to the data used for the interpolation.

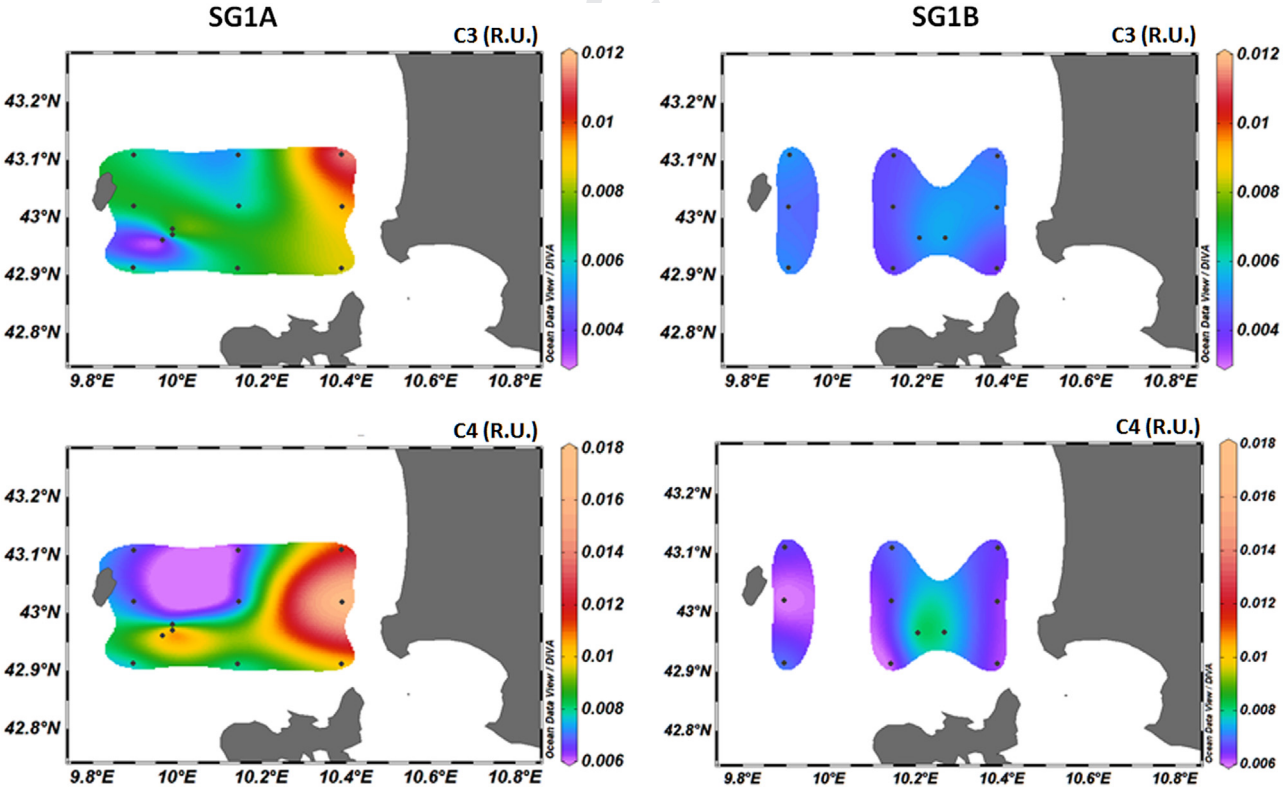

Fig. 12. Surface distributions of "terrestrial" humic-like (C3) and "marine" humic-like (C4) components in the two cruises. The black points refer to the data used for the interpolation.

Acknowledgments

This work was supported by the Med Programme project MEDESS-4MS (Ref: 4175/2S-MED11-01) co-financed by the European Regional Development Funds, by the Italian Flagship Project RITMARE financed by the Italian Ministry for Research – MIUR (PNR 2011-2013, approved by CIPE with adjudication 2/2011 on 23/03/2011) and by the PERSEUS project, funded by the

European Commission under Seventh Framework Program Theme "Oceans of Tomorrow" OCEAN.2011-3, Grant agreement no. 287600. Particular thanks are due to the Italian Coast Guard for having made available vessels and for their assistance and continuous support during the Serious Game exercise.

References

Baker, A., 2001. Fluorescence excitation-emission matrix characterization of some sewage-impacted rivers. Environ. Sci. Technol. 35 (5), 948–953.

Bianchi, T.S., Osburn, C., Shields, M.R., Yvon-Lewis, S., Young, J., Guo, L.D., Zhou, Z.Z., 2014. Deepwater Horizon Oil in Gulf of Mexico Waters after 2 Years: transformation into the Dissolved Organic Matter Pool. Environ. Sci. Technol. 48, 9288–9297.

Berto, D., Giani, M., Savelli, F., Centanni, E., Ferrari, C.R., Pavoni, B., 2010. Winter to spring variations of chromophoric dissolved organic matter in a temperate estuary (Po River, northern Adriatic Sea). Mar. Environ. Res. 70 (1), 73–81.

Carlson, R.E., Fritsch, F.N., 1989. An algorithm for monotone piecewise bicubic interpolation. SIAM J. Numer. Anal. 26, 230–238.

Chin, Y.P., Aiken, G., Oloughlin, E., 1994. Molecular-weight, polydispersity, and spectroscopic properties of aquatic humic substances. Environ. Sci. Technol. 28, 1853–1858.

Christensen, J.H., Hansen, A.B., Mortensen, J., Andersen, O., 2005. Characterization and matching of oil samples using fluorescence spectroscopy and parallel factor analysis. Anal. Chem. 77, 2210–2217.

Coble, P.G., 1996. Characterization of marine and terrestrial DOM in seawater using excitation emission matrix spectroscopy. Mar. Chem. 51, 325–346.

D'Sa, E., Overton, E.B., Lohrenz, S.E., Maiti, K., Turner, R.E., Freeman, A., 2016. Changing dynamics of dissolved organic matter fluorescence in the Northern Gulf of Mexico following the DwH oil spill. Environ. Sci. Technol.

Das, N., Chandran, P., 2010. Microbial degradation of petroleum hydrocarbon contaminants: an overview. Biotechnol. Res. Int. 2011

De Dominicis, M., Bruciaferri, D., Gerin, R., Pinardi, N., Poulain, P.M., Garreau, P., Zodiatis, G., Perivoliotis, L., Fazioli, L., Sorgente, R., 2016. A multi-model assessment of the impact of currents, waves and wind in modelling surface drifters and oil spill. Deep.-Sea Res. Part II http://dx.doi.org/10.1016/j.dsr2.xxxx.xx.xxx this issue.

EEA (European Environment Agency), 2006. Priority issues in the Mediterranean environment. EEA Report. no. 4, 88.

Ferretto, N., Tedetti, M., Guigue, C., Mounier, S., Redon, R., Goutx, M., 2014. Identification and quantification of known polycyclic aromatic hydrocarbons and pesticides in complex mixtures using fluorescence excitation-emission matrices and parallel factor analysis. Chemosphere.

Fichot, C.G., Benner, R., 2012. The spectral slope coefficient of chromophoric dissolved organic matter ($S_{275-295}$) as a tracer of terrigenous dissolved organic carbon in river-influenced ocean margins. Limnol. Oceanogr. 57, 1453–1466.

Gabor, R.S., McKnight, D.M., Miller, M.P., 2014. Fluorescence Indices and Their Interpretation in Aquatic Organic Matter Fluorescence. Cambridge University Press, pp. 303–338.

Gonnelli, M., Vestri, S., Santinelli, C., 2013. Chromophoric dissolved organic matter and microbial enzymatic activity. A biophysical approach to understand the marine carbon cycle. Biophys. Chem. 182, 79–85.

Hansell, D.A., 2005. Dissolved organic carbon reference material program. Eos, Trans. Am. Geophys. Union 86 (35) 318-318.

Hansell, D.A., 2013. Recalcitrant dissolved organic carbon fractions. Mar. Sci., 5.

Helms, J.R., Stubbins, A., Ritchie, J.D., Minor, E.C., Kieber, D.J., Mopper, K., 2008. Absorption spectral slopes and slope ratios as indicators of molecular weight, source, and photobleaching of chromophoric dissolved organic matter. Limnol. Oceanogr. 53, 955–969.

Hong, Y., Wetzel, D., Pulster, E.L., Hull, P., Reible, D., Hwang, H.-M., Ji, P., Rifkin, E., Bouwer, E., 2015. Significant spatial variability of bioavailable PAHs in water column and sediment porewater in the Gulf of Mexico 1year after the Deepwater Horizon oil spill. Environ. Monit. Assess. 187 646–646.

Kvenvolden, K.A., Cooper, C.K., 2003. Natural seepage of crude oil into the marine environment. Geo-Mar. Lett. 23 (3–4), 140–146.

Jorgensen, L., Stedmon, C.A., Kragh, T., Markager, S., Middelboe, M., Sondergaard, M., 2011. Global trends in the fluorescence characteristics and distribution of marine dissolved organic matter. Mar. Chem. 126, 139–148.

Kowalczuk, P., Cooper, W.J., Whitehead, R.F., Durako, M.J., Sheldon, W., 2003. Characterization of CDOM in an organic-rich river and surrounding coastal ocean in the South Atlantic Bight. Aquat. Sci. 65 (4), 384–401.

Kowalczuk, P., Durako, M.J., Young, H., Kahn, A.E., Cooper, W.J., Gonsior, M., 2009. Characterization of dissolved organic matter fluorescence in the South Atlantic Bight with use of PARAFAC model: interannual variability. Mar. Chem. 113, 182–196.

IMO, 1998. Manual on Oil Pollution: IMO Guidelines for Sampling and Identification of Oil Spills, Front Cover. IMO Publishing, p. 38.

Lakowicz, J.R., 2006. Principles of Fluorescence Spectroscopy, 3 ed. Springer, US.

Lawaetz, A.J., Stedmon, C.A., 2009. Fluorescence intensity calibration using the raman scatter peak of water. Appl. Spectrosc. 63, 936–940.

Liu, X., Zhang, Y., Shi, K., Zhu, G., Xu, H., Zhu, M., 2014. Absorption and fluorescence properties of chromophoric dissolved organic matter: implications for the monitoring of water quality in a large subtropical reservoir. Environ. Sci. Pollut. Res. 21 (24), 14078–14090.

Lønborg, C., Álvarez-Salgado, X.A., 2014. Tracing dissolved organic matter cycling in the eastern boundary of the temperate North Atlantic using absorption and fluorescence spectroscopy. Deep. Sea Res. Part I: Ocean. Res. Pap. 85, 35–46.

Mendoza, W.G., Riemer, D.D., Zika, R.G., 2013. Application of fluorescence and PARAFAC to assess vertical distribution of subsurface hydrocarbons and dispersant during the Deepwater Horizon oil spill. Environ. Sci.-Process. Impacts 15, 1017–1030.

Murphy, K.R., Stedmon, C.A., Waite, T.D., Ruiz, G.M., 2008. Distinguishing between terrestrial and autochthonous organic matter sources in marine environments using fluorescence spectroscopy. Mar. Chem. 108, 40–58.

Nelson, N.B., Siegel, D.A., Michaels, A.F., 1998. Seasonal dynamics of colored dissolved material in the Sargasso Sea. Deep. Sea Res. Part I: Ocean. Res. Pap. 45 (6), 931–957.

Para, J., Coble, P.G., Charrière, B., Tedetti, M., Fontana, C., Sempéré, R., 2010. Fluorescence and absorption properties of chromophoric dissolved organic matter (CDOM) in coastal surface waters of the northwestern Mediterranean Sea, influence of the Rhône River. Biogeosciences 7 (12), 4083–4103.

Peuravuori, J., Pihlaja, K., 1997. Pyrolysis electron impact mass spectrometry in studying aquatic humic substances. Anal. Chim. Acta 350, 241–247.

Ramirez, C.E., Wang, C., Gardinali, P.R., 2014. Fully automated trace level determination of parent and alkylated PAHs in environmental waters by online SPE-LC-APPI-MS/MS. Anal. Bioanal. Chem. 406 (1), 329–344.

Ramos-Dorta, C.V., Pino, V., Afonso, A.M., 2013. Monitoring polycyclic aromatic hydrocarbons in seawaters and wastewaters using a dispersive liquid–liquid microextraction method. Environ. Technol. 34 (5), 607–616.

Retelletti Brogi, S., Gonnelli, M., Vestri, S., Santinelli, C., 2015. Biophysical processes affecting DOM dynamics at the Arno river mouth (Tyrrhenian Sea). Biophys. Chem. 197, 1–9.

Santinelli, C., 2015. DOC in the Mediterranean Sea, Biogeochemistry of Marine Dissolved Organic Matter. Academic Press Elsevier, Burlington, pp. 579–608.

Seritti, A., Russo, D., Nannicini, L., Del Vecchio, R., 1998. DOC, absorption and fluorescence properties of estuarine and coastal waters of the Northern Tyrrhenian Sea. Chem. Speciat. Bioavailab. 10 (3), 95–106.

Sorgente, R., Tedesco, C., Pessini, F., De Dominicis, M., Gerin, R., Olita, A., Fazioli, L., Di Maio, A., Ribotti, A., 2016. Forecast of drifter trajectories using a Rapid Environmental Assessment based on CTD observations. Deep-Sea Res. Part II, (this issue) http://dx.doi.org/[10.1016/j.dsr2.xxxx.xx.xxx].

Stedmon, C.A., Markager, S., Kaas, H., 2000. Optical properties and signatures of chromophoric dissolved organic matter (CDOM) in Danish coastal waters. Estuar., Coast. Shelf Sci. 51 (2), 267–278.

Stedmon, C.A., Bro, R., 2008. Characterizing dissolved organic matter fluorescence with parallel factor analysis: a tutorial. Limnol. Oceanogr.-Methods 6, 572–579.

Stedmon, C.A., Markager, S., 2005. Resolving the variability in dissolved organic matter fluorescence in a temperate estuary and its catchment using PARAFAC analysis. Limnol. Oceanogr. 50, 686–697.

Stedmon, C., Nelson, N.B., 2015. The optical properties of DOM in the ocean, Biogeochemistry of Marine Dissolved Organic Matter. Elsevier Science.

Tedetti, M., Longhitano, R., Garcia, N., Guigue, C., Ferretto, N., Goutx, M., 2012. Fluorescence properties of dissolved organic matter in coastal Mediterranean waters influenced by a municipal sewage effluent (Bay of Marseilles, France). Environ. Chem. 9 (5), 438–449.

Zengel, S., Bernik, B.M., Rutherford, N., Nixon, Z., Michel, J., 2015. Heavily oiled salt marsh following the deepwater horizon oil spill, ecological comparisons of shoreline cleanup treatments and recovery. Plos One, 10.

Zeri, C., Beşiktepe, Ş., Giannakourou, A., Krasakopoulou, E., Tzortziou, M., Tsoliakos, D., Pavlidou, A., Mousdid, G., Pitta, E., Scoullos, M., Papathanassiou, E., 2014. Chemical properties and fluorescence of DOM in relation to biodegradation in the interconnected Marmara–North Aegean Seas during August 2008. J. Mar. Syst. 135, 124–136.

Zhou, Z.Z., Guo, L.D., Shiller, A.M., Lohrenz, S.E., Asper, V.L., Osburn, C.L., 2013. Characterization of oil components from the Deepwater Horizon oil spill in the Gulf of Mexico using fluorescence EEM and PARAFAC techniques. Mar. Chem. 148, 10–21.

Ziervogel, K., McKay, L., Rhodes, B., Osburn, C.L., Dickson-Brown, J., Arnosti, C., Teske, A., 2012. Microbial activities and dissolved organic matter dynamics in oil-contaminated surface seawater from the Deepwater Horizon oil spill site. Plos One 7 (4), e34816.

Please cite this article as: Gonnelli, M, et al., Dissolved organic matter dynamics in surface waters affected by oil spill pollution: Results from the Serious Game exercise. Deep-Sea Res. II (2016), http://dx.doi.org/10.1016/j.dsr2.2016.05.027